Available online at www.sciencedirect.com
SCIENCE DIRECT®
Journal of Computational Physics 200 (2004) 489–511
JOURNAL OF COMPUTATIONAL PHYSICS
www.elsevier.com/locate/jcp

Stokes eigenmodes in square domain and the stream function–vorticity correlation

E. Leriche *, G. Labrosse [1]

Laboratoire d'Ingénierie Numérique, Institut des Sciences de l'Energie, Faculté des Sciences et Technique de l'Ingénieur, Ecole Polytechnique Fédérale de Lausanne, CH-1015 Ecublens, Switzerland

Received 10 June 2003; received in revised form 9 March 2004; accepted 10 March 2004
Available online 10 June 2004

Abstract

The Stokes eigenmodes in the square are numerically determined and their symmetry properties are identified. The spectra evolution laws are in excellent qualitative agreement with the theoretical asymptotic predictions proposed by Constantin and Foias (in "Navier–Stokes equations", University of Chicago Press, 1988), $\lambda_k \simeq k + \mathcal{O}(\sqrt{k})$. The slopes are reported here and are found to be specific to the eigenmodes symmetry family. The dynamic equilibria are analyzed and show a linear relationship between the vorticity and the stream function in the core of the eigenmodes. These features of the Stokes eigenmodes confined in the square are shared by the fully periodic Stokes eigenmodes.

1. Introduction

Why to study the Stokes eigenmodes, whereas nonlinear dynamics is the most attractive part of the Navier–Stokes equations? The dynamical behaviors governed by the Navier–Stokes equations result from the way this nonlinear dynamics is controlled by diffusion. For instance, in isothermal mono-component fluid, turbulence can be primarily seen as resulting from an imbalance between the $(\mathbf{u}\cdot\nabla)\mathbf{u}$ and $\Delta\mathbf{u}$ contributions. No internal length scale can be found to put these terms in equilibrium. Understanding then the intrinsic dynamics of the diffusion part of Navier–Stokes can supply an interesting point of view on turbulence.

Since the early work of Taylor [35] on the leading eigenmode of the buckling load problem, only a few attempts have been made to compute few Stokes eigenvalues and/or eigenmodes in fully confined geometries [5–11,13,36–38]. Apart from the theoretical predictions proposed in [14] on the asymptotic behavior

* Corresponding author.
E-mail addresses: emmanuel.leriche@epfl.ch (E. Leriche), labrosse@limsi.fr (G. Labrosse).
[1] On leave from Université Paris-Sud, LIMSI-CNRS, BP 133, 91403 Orsay Cedex, France.

0021-9991/$ - see front matter
doi:10.1016/j.jcp.2004.03.017

of the eigenvalues in 2D or 3D confined domains, there is as yet no global view of the Stokes eigenspace in the square. This is because Stokes eigenmodes in confined geometries are not easily accessible.

Numerically determining the confined Stokes eigenmodes is not an easy task. The choice made for uncoupling the pressure from the velocity fields is crucial for the consistency and computational complexity of the scheme. For instance, in [5] a Uzawa uncoupling method is applied for computing the eigenmodes of the generalized singular Stokes problem in order to provide a basis for the channel and grooved channel flows. This approach – already expensive in 2D – practically excludes access to 3D eigenmodes. To the authors' point of view, the projection-diffusion (PrDi) uncoupling [20], which is also consistent with the continuous problem [22] but optimal in computation cost, allows the 2D/3D eigenmodes to be computed.

The scope of the present work is to provide the first deep insight into the Stokes eigenspace in the square. The eigenvalues and eigenmodes are accurately computed by two different means, namely, a Chebyshev PrDi solver and a Galerkin–Reid–Harris (RH) expansion of the stream function. The symmetries which underlie the eigenmode patterns are also identified. The evolution laws of the spectra were fitted. They qualitatively agree with the theoretical estimations proposed in [14]. An analysis of the peculiar dynamics of the eigenmodes is also performed. Each symmetry family exhibits its own spectrum slopes. Furthermore, a linear relationship between the vorticity and the stream function is inferred from the dynamic equilibria at the core of each eigenmode. Frequent references are made to the fully periodic Stokes eigenspace features.

Confined 2D flows can thus be characterized by functional relationships between the vorticity and the stream function not only in the inviscid regions at high Reynolds number [4].

2. Outline

The paper is organized as follows. The governing equations are first presented in Section 3 for the various Stokes formulations. In view of further comparisons, Section 4 recalls the analytical expressions of the Stokes eigenmodes which are periodic in all, and in all but one, space directions. Section 5 presents the symmetry families of the Stokes eigenmodes in the square. Section 6 presents the solvers. Since corner eddies are expected to be part of each eigenmode, Section 7 makes a brief survey of their properties. Finally, the results are presented in Section 8, followed by a conclusion.

3. Governing equations

Let us write the dimensionless unsteady (time t) 2D Stokes equations, with primitive variables, in the open domain $\Omega =]-1,1[^2$ with coordinates $\mathbf{x} = (x,y)$ and T a real positive number:

$$\begin{aligned} &\frac{\partial \mathbf{u}}{\partial t} = \Delta \mathbf{u} - \nabla p + \mathbf{f} \quad \text{for} \quad (\mathbf{x},t) \in \Omega \times]0,T[, \\ &\nabla \cdot \mathbf{u} = 0 \quad \text{for} \quad (\mathbf{x},t) \in \Omega \times]0,T[, \end{aligned} \tag{1}$$

where $\mathbf{u} = (u,v)$ is the velocity field, p the pressure and $\mathbf{f}$ a source term. We denote the closure of Ω by $\overline{\Omega}$ and the boundary by $\partial\Omega$. Dirichlet boundary conditions are imposed on the velocity

$$\mathbf{u} = \mathbf{V} \quad \text{for} \quad (\mathbf{x},t) \in \partial\Omega \times]0,T[,$$

and compatible initial conditions are given

$$\mathbf{u}(t=0) = \mathbf{V}^0 \quad \text{for} \quad \mathbf{x} \in \Omega.$$

3.1. The Stokes eigenproblem in primitive variables

The eigenproblem is defined by $\partial\mathbf{u}/\partial t = \lambda\mathbf{u}$ together with $\mathbf{f} = 0 = \mathbf{V}$, λ being thus the algebraic temporal growth rate of $\mathbf{u}$. The eigensystem reads as follows:

$$\begin{aligned} &\lambda\mathbf{u} = \boldsymbol{\Delta}\mathbf{u} - \nabla p \quad \text{for} \quad \mathbf{x} \in \Omega, \\ &\nabla \cdot \mathbf{u} = 0 \quad \text{for} \quad \mathbf{x} \in \Omega, \\ &\mathbf{u} = \mathbf{0} \quad \text{for} \quad \mathbf{x} \in \partial\Omega. \end{aligned} \tag{2}$$

3.2. The Stokes eigenproblem in stream function formulation

An alternative form of the system of Eq. (2) is its stream function formulation, known in structural mechanics as the buckling load problem [28,35]. It is based on $\psi(\mathbf{x})$ such that $(u, v) = (\partial\psi/\partial y, -\partial\psi/\partial x)$, and reads

$$(\lambda - \boldsymbol{\Delta})\boldsymbol{\Delta}\psi = 0 \quad \text{for} \quad \mathbf{x} \in \Omega \tag{3}$$

with homogeneous no-slip/no-flux boundary conditions

$$\psi = \frac{\partial\psi}{\partial n} = 0 \quad \text{for } \mathbf{x} \in \partial\Omega, \tag{4}$$

n being the coordinate evaluated along $\mathbf{n}$, the outward unit vector normal to $\partial\Omega$.

4. The presently known Stokes eigenmodes

This paper concerns the Stokes eigenmodes in the square. To the authors' knowledge, the Cartesian Stokes eigenmodes are not analytically known except when they are periodic in all, or in all but one, space directions. If they are indeed constrained to satisfy velocity no-slip conditions on a closed boundary they can only be determined by a numerical approach. For future reference a brief survey of the analytically known Cartesian eigenmodes is provided in this section.

4.1. The fully periodic Stokes eigenmodes

Starting from Eq. (1) the fully periodic solutions of the Stokes problem

$$\begin{pmatrix} \mathbf{u} \\ p \end{pmatrix} = \begin{pmatrix} \tilde{\mathbf{u}} \\ \tilde{p} \end{pmatrix} \mathrm{e}^{\mathrm{i}(\mathbf{k}\cdot\mathbf{x}+\omega t)}$$

are associated with a periodic source term $\mathbf{f} = \tilde{\mathbf{f}}\mathrm{e}^{\mathrm{i}(\mathbf{k}\cdot\mathbf{x}+\omega t)}$, where $(\tilde{\mathbf{u}}, \tilde{p}, \tilde{\mathbf{f}})$ are complex Fourier coefficients, and $\mathbf{k}$ the wavevector. The solution reads

$$\tilde{p} = -\mathrm{i}\frac{\hat{\mathbf{k}}\cdot\tilde{\mathbf{f}}}{k}, \quad (\mathrm{i}\omega + k^2)\tilde{\mathbf{u}} = [\tilde{\mathbf{f}} - \hat{\mathbf{k}}(\hat{\mathbf{k}}\cdot\tilde{\mathbf{f}})],$$

where $\hat{\mathbf{k}}$ is the unit vector along $\mathbf{k}$ and $\mathbf{k} = k\hat{\mathbf{k}}$. The fully periodic eigenmode ($\lambda = \mathrm{i}\omega$) is therefore defined by

$$\tilde{p} = 0, \quad (\lambda + k^2)\tilde{\mathbf{u}} = 0, \quad \hat{\mathbf{k}}\cdot\tilde{\mathbf{u}} = 0. \tag{5}$$

It is thus important to notice that the periodic Stokes eigenmodes are pure isobaric ($p = 0$) diffusion modes, with $\lambda = -k^2$. Moreover the constraint $\nabla \cdot \mathbf{u} = 0$ does not affect their spatial structure, but only requires the wavevector $\hat{\mathbf{k}}$ to be transverse to the velocity.

4.2. The 1D confined Stokes eigenmodes

The 1D confined (in x) Stokes eigenmodes are presented in detail in [25]. They are expressed according to

$$\begin{pmatrix} \mathbf{u} \\ p \end{pmatrix} = \begin{pmatrix} \tilde{\mathbf{u}}(x) \\ \tilde{p}(x) \end{pmatrix} \mathrm{e}^{\mathrm{i}ky+\lambda t},$$

where k is a wavenumber and $(\tilde{\mathbf{u}}(x), \tilde{p}(x))$ are complex functions. The stream functions of the eigenmodes are either symmetric or anti-symmetric in x, with their eigenvalues $\lambda = -(k^2 + \mu^2)$, respectively, obtained from

$$\mu_{\mathrm{even}} \tan(\mu_{\mathrm{even}}) = -k \tanh(k), \quad \mu_{\mathrm{odd}} \cot(\mu_{\mathrm{odd}}) = k \coth(k).$$

The first eigenvalues are listed in [25] for $k = 1, 10$.

5. Symmetries

Apart from translation, which is not of interest here, two planar isometries will be considered [32]. Firstly, the θ-rotation. Secondly, the (D)-symmetry which is the reflection about the straight line (D) making an angle $\alpha/2$ with the unit horizontal axis $\hat{\mathbf{e}}_x$ (Fig. 1). Let us successively denote $\mathscr{R}(\theta)$ and $\mathscr{S}(\alpha)$ as the operators which describe these transformations, and $|\Psi(M)\rangle$ a state (defined below) known as a scalar function $\Psi(x, y)$. One will have $|\Psi(M')\rangle = \mathscr{R}(\theta)|\Psi(M)\rangle$ and $|\Psi(M'')\rangle = \mathscr{S}(\alpha)|\Psi(M)\rangle$ the new states, respectively obtained after rotation and (D)-symmetry applied on $|\Psi(M)\rangle$. The respective coordinate transformations are

$$\begin{pmatrix} x' \\ y' \end{pmatrix} = \begin{pmatrix} \cos(\theta) & -\sin(\theta) \\ \sin(\theta) & \cos(\theta) \end{pmatrix} \begin{pmatrix} x \\ y \end{pmatrix},$$

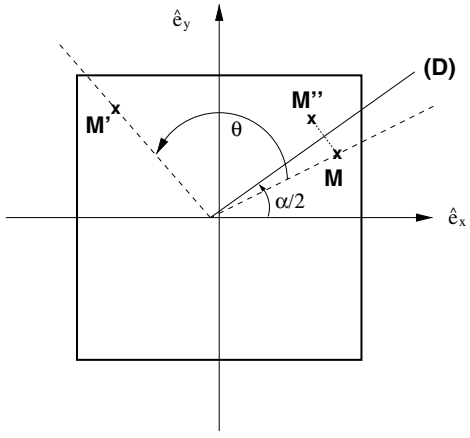

Fig. 1. θ-Rotation and reflection about a straight line (D) making an angle $\alpha/2$ with $\hat{\mathbf{e}}_x$.

and

$$\begin{pmatrix} x'' \\ y'' \end{pmatrix} = \begin{pmatrix} \cos(\alpha) & \sin(\alpha) \\ \sin(\alpha) & -\cos(\alpha) \end{pmatrix} \begin{pmatrix} x \\ y \end{pmatrix}.$$

Composition rules are easy to establish, for instance

$$\mathscr{R}(\theta_1)\mathscr{R}(\theta_2) = \mathscr{R}(\theta_1 + \theta_2),$$

$$\mathscr{R}(\theta)\mathscr{S}(\alpha) = \mathscr{S}(\theta + \alpha), \quad \mathscr{S}(\alpha)\mathscr{R}(\theta) = \mathscr{S}(\alpha - \theta),$$

$$\mathscr{S}(\alpha_1)\mathscr{S}(\alpha_2) = \mathscr{R}(\alpha_1 - \alpha_2),$$

which leads to the following identity relations:

$$(\mathscr{R}(\theta))^2 = 1 \quad \text{if } \theta = n\pi,\ |n| = 0, 1, \ldots \quad \text{and} \quad (\mathscr{S}(\alpha))^2 = 1 \quad \forall\alpha.$$

It follows:
(a) If $\mathscr{R}(\pi)|\Psi\rangle = \xi|\Psi\rangle$, one has necessarily $\xi = \pm 1$.
(b) If $|\Psi\rangle$ verifies $\mathscr{R}(\frac{\pi}{2})|\Psi\rangle = \xi|\Psi\rangle$, one has necessarily $\mathscr{R}(\pi)|\Psi\rangle = |\Psi\rangle$, and $\xi = \pm 1$.
(c) If $\mathscr{S}(\alpha)|\Psi\rangle = \xi|\Psi\rangle$, one has necessarily $\xi = \pm 1\ \forall\alpha$.
In the square the angles α and θ are quantified as integer multiples of $\pi/2$. A total of four rotations and four (D)-symmetries are thus possible in this domain. These are generated by only three independent transformations, chosen here as being $\mathscr{R}(\pi)$, $\mathscr{R}(\frac{\pi}{2})$ and $\mathscr{S}(0)$, whose common eigenmodes span the functional space of any Stokes solution. Let us note $|\xi_1, \xi_2, \xi_3\rangle$ these eigenmodes thus defined by the following three relations:

$$\mathscr{R}(\pi)|\xi_1, \xi_2, \xi_3\rangle = \xi_1|\xi_1, \xi_2, \xi_3\rangle,$$
$$\mathscr{R}\left(\frac{\pi}{2}\right)|1, \xi_2, \xi_3\rangle = \xi_2|1, \xi_2, \xi_3\rangle,$$
$$\mathscr{S}(0)|\xi_1, \xi_2, \xi_3\rangle = \xi_3|\xi_1, \xi_2, \xi_3\rangle,$$

in which we have $\xi_1 = \pm 1$, $\xi_3 = \pm 1$ and $\xi_2 = \pm 1$ only with $\xi_1 = 1$. The $\xi_1 = -1$ states have no $\mathscr{R}(\pi/2)$ symmetry. They are denoted by $|-1, /, \pm 1\rangle$. Together with the $|1, \pm 1, \pm 1\rangle$ states, we have therefore six symmetry families for classifying the Stokes solutions. Those having given ξ_2 and ξ_3 are also eigenmodes of $\mathscr{S}((2n+1)(\pi/2))$, representing reflection about the square diagonals with $\xi_2\xi_3$ as eigenvalue. Therefore, in contrast with the others, the families $|-1, /, \pm 1\rangle$ have no reflection symmetry about the square diagonals. Finally, from the relations

$$\mathscr{R}\left(\frac{\pi}{2}\right)|-1, /, \pm 1\rangle = \pm|-1, /, \mp 1\rangle$$

it is inferred that the Stokes eigenmodes which are odd under the π-rotation appear by pair associated with the same eigenvalue.

6. Solvers

Computing the Stokes eigenmodes can be made from either their (velocity–pressure) primitive variables or stream function formulation, but the choice of the scheme is particularly relevant. For instance, one of the problems raised by the accurate numerical determination of the eigenmodes regards the possible

requirement of enforcing the numerical velocity to be divergence free in order to obtain relevant and convergent results.

With the former formulation, the well-known Stokes solvers are either non-consistent, namely the time-splitting schemes, or very expensive even for the 2D present case, namely the Uzawa [2,27] and Green (or influence matrix) [19] options. On the stream function formulation side, an interesting Galerkin–Legendre or –Chebyshev approach is proposed in [30,31] for solving the fourth order scalar elliptic equation. It has been used in [8,9,36] for computing the very first buckling load eigenmodes. It is worth mentioning here that the biorthogonal series based on "Papkovich-Fadle" polynomial expansions [16,29,33] cannot be used for solving this problem. They lead indeed to a transcendental eigenvalue system, the matrix entries depending on the eigenvalue to evaluate [34].

The present work is based on two different spectral expansions, associated with each Stokes formulation: a Chebyshev polynomial expansion and the Galerkin–RH decomposition. The former one feeds a pseudo-spectral solver in primitive variables (the PrDi) known to be consistent with the continuous space–time problem [22] and optimal in computation cost. The latter one with easy implementation, uses the well-known no-slip/no-flux eigenmodes of the fourth-order differential problem [18,26] for directly solving the stream function formulation. These approaches are quite different, as regards, for instance, the numerical velocity. In the former case the divergence is allowed to vanish (see Section 6.1.1) but only asymptotically with the cut-off frequency whilst for the latter case it is exactly zero. The RH approach will play an assessment role for this aspect of the problem, and also help in the interpretation and in completion of the PrDi results. A systematic comparison of the numerical convergence of PrDi and RH solutions is provided in [23].

6.1. Formulation in velocity–pressure variables

The unsteady Stokes problem is solved with a PrDi solver which uncouples the $(\mathbf{u}, p)$ fields independently of any temporal scheme. Section 3.2 in [22] provides all the details about the discrete formulation of the problem, which this section relies on. The spatial discretization is based on the usual Chebyshev Gauss–Lobatto collocation method [17,12]. Let N be the polynomial cut-off frequency, where $N+1$ is the number of collocation points, in each space direction. For the sake of conciseness, the equations in this subsection are written as the continuous transposition of the corresponding discrete problem, with for instance $\nabla\cdot$ standing for the discrete $(N+1)^2$ divergence operator and $\mathbf{x}\in\Omega$ meaning that only the internal nodes are concerned.

From the first equation (2), an intermediate divergence free field is introduced, the acceleration $\mathbf{a}$,

$$\mathbf{a} = \lambda\mathbf{u} - \Delta\mathbf{u} \quad \text{for } \mathbf{x}\in\overline{\Omega}$$

and the problem is solved through two steps.

(1) The pressure is evaluated from

$$\begin{aligned} &\mathbf{a} + \nabla p = 0 \quad \text{for } \mathbf{x}\in\ \Omega_i \quad (i=1,2),\\ &\nabla\cdot\mathbf{a} = 0 \quad \text{for } \mathbf{x}\in\ \overline{\Omega}\\ &\mathbf{a}\cdot\mathbf{n} = (\nabla\times\nabla\times\mathbf{u})\cdot\mathbf{n} \quad \text{for } \mathbf{x}\in\partial\Omega, \end{aligned} \tag{6}$$

where

$$\begin{aligned} \Omega_1 &=]-1,+1[\times[-1,+1],\\ \Omega_2 &= [-1,+1]\times]-1,+1[\end{aligned}$$

for the respective components of the first equation in (6).

It is important to mention here the following equivalent ($N \to \infty$) numerical version of this step (see Sections 3.2 and 4.2 in [22])

$$\begin{aligned} &\Delta p = 0 \quad \text{for } \mathbf{x} \in \Omega, \\ &\frac{\partial p}{\partial n} = -(\nabla \times \nabla \times \mathbf{u}) \cdot \mathbf{n} \quad \text{for } \mathbf{x} \in \partial\Omega. \end{aligned} \tag{7}$$

(2) Then the velocity is evaluated through the diffusion step

$$\begin{aligned} &\lambda \mathbf{u} - \Delta \mathbf{u} = \mathbf{a} \quad \text{for } \mathbf{x} \in \Omega, \\ &\mathbf{u} = 0 \quad \text{for } \mathbf{x} \in \partial\Omega. \end{aligned} \tag{8}$$

6.1.1. About the solenoidality of the numerical eigenmodes

The system (6) of the pressure step provides a numerical field **a** whose divergence exactly cancels at all the nodes, boundaries included, whereas by Eq. (7) this divergence vanishes only on the internal nodes. However, the truncation of the diffusion step (8) prevents, in both cases, the resulting velocity from being solenoidal, but asymptotically with the cut-off frequency, if this field verifies the required regularity conditions. As a consequence, the eigenmodes of both equivalent versions of this solver (6)–(8), or (7) and (8) cannot be exactly divergence free. It is then worth preparing the interpretation of the results by predicting the main features of the forthcoming eigenmodes. By Eqs. (6)–(8) or (7) and (8), the numerical eigenmodes verify the relation

$$\lambda \mathbf{u} = \nabla(\nabla \cdot \mathbf{u}) - \nabla \times \nabla \times \mathbf{u} - \nabla p \quad \text{for } \mathbf{x} \in \overline{\Omega}, \tag{9}$$

which, applied onto the boundaries where $\mathbf{u} = 0$, implies that

$$0 = \nabla(\nabla \cdot \mathbf{u}) - \nabla \times \nabla \times \mathbf{u} - \nabla p \quad \text{for } \mathbf{x} \text{ on } \partial\Omega. \tag{10}$$

Two distinct cases are now encompassed:

(1) The PrDi eigenmode is asymptotically divergence free. It is therefore a candidate for a genuine Stokes eigenmode, and it must verify, to a good accuracy, at all the nodes on the boundary the relation

$$\nabla p = -\nabla \times \nabla \times \mathbf{u} \equiv \Delta \mathbf{u} \quad \text{for } \mathbf{x} \text{ on } \partial\Omega. \tag{11}$$

For this eigenmode category, it makes sense to define a stream function $\psi(\mathbf{x})$ solution of the vorticity relationship $\omega(\mathbf{x}) \equiv \partial v/\partial x - \partial u/\partial y = -\Delta\psi$, with $\psi = 0$ on the boundary where it also verifies the zero flux condition.

(2) The PrDi eigenmode is not asymptotically divergence free. Applying then the divergence to Eq. (9), and taking into account both relations (7) lead to the corresponding characteristic relations

$$\begin{aligned} &\lambda(\nabla \cdot \mathbf{u}) = \Delta(\nabla \cdot \mathbf{u}) \quad \text{for } \mathbf{x} \in \Omega, \\ &\frac{\partial}{\partial n}(\nabla \cdot \mathbf{u}) = 0 \quad \text{for } \mathbf{x} \in \partial\Omega. \end{aligned} \tag{12}$$

Modes with finite divergence are thus allowed to exist in the numerical system, but as eigenmodes of the divergence diffusion, with a spectrum corresponding to zero divergence flux boundary conditions. Their eigenvalues are multiple integers of $(-\pi^2/4)$, excluding $\lambda = 0$ which would imply $\nabla \cdot \mathbf{u} = 0$.

6.1.2. The discrete Stokes operator

The expression of the discrete Stokes operator as well as preliminary results on its spectrum are given in Section 4.1 of [22]. A brief presentation of this operator is made now.

Its expression is the direct numerical translation of $\lambda\mathbf{u} = \Delta\mathbf{u} - \nabla p$. Denoting by $\mathbf{U}$ the column vector, of $(N-1)^2$ entries, the internal nodal values of $\mathbf{u}$ (it vanishes on the boundary), the time evolution discrete-in-space operator $\mathscr{L}$ reads

$$\lambda\mathbf{U} = \mathscr{L}\mathbf{U} \equiv (\mathscr{A}_{\mathrm{D}} + \mathscr{B})\mathbf{U}. \tag{13}$$

The first part of $\mathscr{L}$ is the diffusion operator, the discrete Laplacian, $\mathscr{A}_{\mathrm{D}}$, defined accordingly with the Dirichlet homogeneous velocity boundary conditions. The second operator, $\mathscr{B}$, brings the contribution of the pressure gradient, obtained from Eq. (6) and fed by the associated boundary conditions. This $\mathscr{B}$ operator handles a reduced number of independent quantities, namely the $4N$ boundary nodal values of $(\nabla \times \nabla \times \mathbf{U}) \cdot \mathbf{n}$, and therefore possesses a large kernel of dimension $(N-1)^2 - 4N$. The genuine Stokes eigenmodes are those which satisfy the relation (11). They are generated by the coupling of $\mathscr{A}_{\mathrm{D}}$ and $\mathscr{B}$ and their number cannot exceed $4N$. They are to be extracted by symmetry family. The remaining $\mathscr{L}$ eigenmodes are of diffusion type, Eq. (12). We therefore see that the coupling between diffusion and the continuity constraint is minimized in Eq. 13, i.e. reduced to accounting for the existence of boundaries, which is not far from what happens in the fully periodic case (see the last two sentences of Section 4.1).

6.2. Stream function formulation

A Galerkin–RH expansion of the stream function is here adopted for solving the system (3) and (4). Let

$$C_i(x) = \frac{1}{\sqrt{2}}\left(\frac{\cosh(\mu_i x)}{\cosh(\mu_i)} - \frac{\cos(\mu_i x)}{\cos(\mu_i)}\right), \quad S_i(x) = \frac{1}{\sqrt{2}}\left(\frac{\sinh(\nu_i x)}{\sinh(\nu_i)} - \frac{\sin(\nu_i x)}{\sin(\nu_i)}\right), \quad i = 1, 2, \ldots$$

be the, respectively, even and odd eigenfunctions of the 1D differential problem

$$\frac{\mathrm{d}^4 f}{\mathrm{d}x^4} = \lambda^4 f, \quad f(x = \pm 1) = 0 = \frac{\mathrm{d}f}{\mathrm{d}x}(x = \pm 1)$$

with the respective eigenvalues μ_i^4 and ν_i^4 roots of

$$\tanh(\mu_i) + \tan(\mu_i) = 0, \quad \coth(\nu_i) - \cot(\nu_i) = 0.$$

The stream function can be looked for as appropriate Galerkin expansions of the 2D tensorial products of these 1D functions. For each symmetry family there exists a simple way to generate functions of x and y which enjoy the desired symmetries. Let $E(x)$ and $O(x)$ represent two functions (possibly endowed with a subscript), respectively, even and odd with respect to their argument, x, for the moment. It can be checked that the analytical representation of the different states is

$$|1, \pm 1, 1\rangle \div E_1(x)E_2(y) \pm E_2(x)E_1(y),$$

$$|1, \pm 1, -1\rangle \div O_1(x)O_2(y) \mp O_2(x)O_1(y),$$

$$|-1, /, 1\rangle \div O(x)E(y),$$

$$|-1, /, -1\rangle \div E(x)O(y).$$

Their Galerkin expansion, in terms of the RH functions, then reads

$$|1,1,1\rangle = \sum_{i \geqslant j=1}^{I} a_{ij}\big[C_i(x)C_j(y) + C_j(x)C_i(y)\big],$$

$$|1,-1,1\rangle = \sum_{i>j=1}^{I} a_{ij}\big[C_i(x)C_j(y) - C_j(x)C_i(y)\big],$$

$$|1,1,-1\rangle = \sum_{i>j=1}^{I} a_{ij}\big[S_i(x)S_j(y) - S_j(x)S_i(y)\big],$$

$$|1,-1,-1\rangle = \sum_{i \geqslant j=1}^{I} a_{ij}\big[S_i(x)S_j(y) + S_j(x)S_i(y)\big],$$

$$|-1,/,1\rangle = \sum_{i,j=1}^{I} a_{ij}S_i(x)C_j(y),$$

$$|-1,/,-1\rangle = \sum_{i,j=1}^{I} a_{ij}C_i(x)S_j(y).$$

Only one of the last two eigenmodes needs to be evaluated, the other being simply deduced by application of $\pi/2$-rotation. They have identical eigenvalues and only five eigenmodes families are thus presented hereafter.

A given I provides I^2 Stokes modes in the family $|-1,/,-1\rangle$, $I(I+1)/2$ Stokes modes $|1,1,1\rangle$ and $|1,-1,-1\rangle$, and $I(I-1)/2$ Stokes modes $|1,-1,1\rangle$ and $|1,1,-1\rangle$.

The stream function $\psi(x,y)$ of each family of eigenmode corresponds to a particular set of a_{ij} coefficients to be computed for verifying Eq. (3).

7. About the singular corner eddies

As is well known since Moffatt's work [24], the Stokes eigenmodes contain an infinite sequence of similar corner eddies, singular at each of the square four corners, verifying $\mathbf{\Delta}^2\psi = 0$ with $\psi = \partial\psi/\partial n = 0$ on the boundaries. They are not specific of the Stokes eigenmodes but of their symmetry: the corner eddies are even about the square diagonals for the families $|1,1,1\rangle$ and $|1,-1,-1\rangle$ (Fig. 2(a)), odd for $|1,-1,1\rangle$ and $|1,1,-1\rangle$ (Fig. 2(b)), and without diagonal symmetry for the last families $|-1,/,\pm1\rangle$ (Fig. 2(c)). The intensity of each eddy decreases exponentially towards the corners. This reduction is much more rapid when the eddies are odd about the square diagonals, that is with the families $|1,-1,1\rangle$ and $|1,1,-1\rangle$. As a consequence, these eddies are mainly even in the families $|-1,/,\pm1\rangle$ (Fig. 2(c)).

Their complete description is supplied in [23], their main characteristics (intensities and position of the corner eddies centers) being pointed out, in each symmetry family, illustrating in this way the different capabilities of both solvers.

These corner eddies provide the major contribution to the divergence of the numerical velocity supplied by the PrDi solver. It is therefore expected that $|\nabla \cdot \mathbf{u}|$ be much smaller for the $|1,-1,1\rangle$ and $|1,1,-1\rangle$ families than for the others, as explained in [23].

In contrast, the diffusion eigenmodes, see Eq. (12), do not contain any corner eddy.

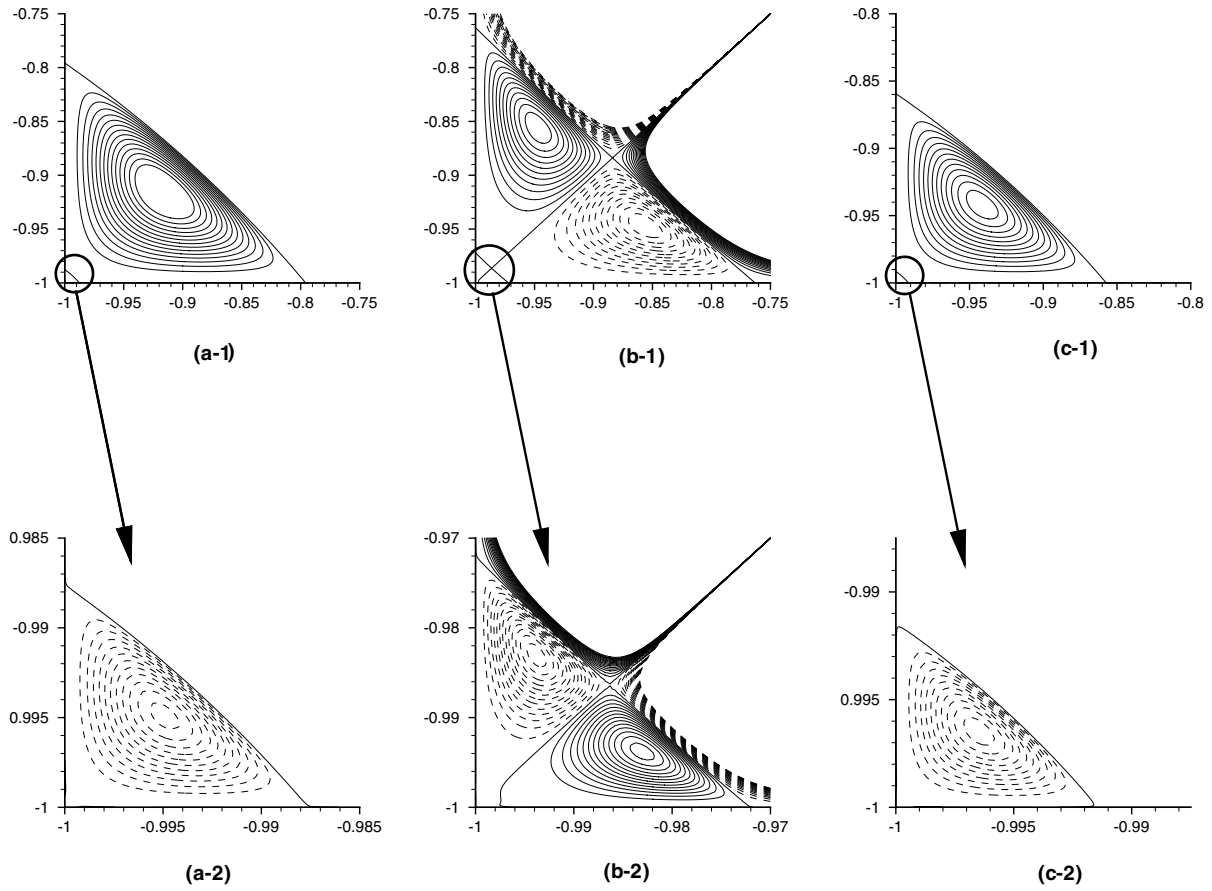

Fig. 2. Enlargements of the $\psi(x,y)$ contour plots of the fundamental $|1,1,1\rangle$, $|1,-1,1\rangle$ and $|-1,/,-1\rangle$ eigenmodes obtained from the $N = 96$ PrDi solver. Solid and dashed lines, respectively, correspond to positive (and zero) and negative levels. The contour levels (15 in (a,c) and 31 in (b)) are evenly distributed in between the following ranges: (a-1): $[0, 10^{-4}]$, (a-2): $[-4 \times 10^{-9}, 0]$; (b-1): $[-2 \times 10^{-5}, 2 \times 10^{-5}]$, (b-2): $[-7 \times 10^{-11}, 7 \times 10^{-11}]$; (c-1): $[0, 9 \times 10^{-5}]$, (c-2): $[-3 \times 10^{-9}, 0]$.

8. Results

The complete $\mathscr{L}$ spectrum is computed (MATLAB software, [1]) with $N = 16$, 32, 48, and only the 200 leading eigenmodes (ARPACK Library, [21]) for $N = 64$, 96. The $N = 96$ results are taken as reference (cf. [23]). The RH eigenvalue systems are solved using the Mathematica software [40]. A significant number of Stokes eigenmodes is computed, in each symmetry family, with the cut-off $I = 15$, 31, 63.

8.1. Convergence and interpretation of the numerical spectra

The convergence of the $\mathscr{L}$ spectrum is reported in Section 4.1, Table 3, in [22], where the 11 largest eigenvalues obtained with $N = 8$, 16, 32, 48 are provided. As also indicated in the same paper, the eigenvalues are spread into two categories with one set containing values converging towards integer mul-

tiples of $(-\pi^2/4)$. From now on the eigenvalues are ordered in each family by increasing absolute value, and denoted by λ_k^N, $k = 1, 2, \ldots$

A first global glance at the convergence of the spectra with N is given in Fig. 3 where the ratios $|(\lambda_k^{96} - \lambda_k^N)/\lambda_k^{96}|$ are plotted, as functions of $-\lambda_k^N/(\pi^2/4)$, for $k \leqslant 200$, with circles whose diameter decreases with increasing N. The exponential convergence clearly appears, with the cloud of smallest circles located at about 10^{-9} and below. Another aspect of this convergence is instructive. With the same symbol conventions, Fig. 4 shows the relative divergence norm, $\|\nabla \cdot \mathbf{u}_k\|/\|\mathbf{u}_k\|$, still as a function of $-\lambda_k^N/(\pi^2/4)$, where $\|\clubsuit\|$ stands for the pointwise maximum absolute value of $\clubsuit$ and $\|\mathbf{u}\| = \max(\|u\|, \|v\|)$. Two different clouds clearly appear, joined by a scattered line of large diameter circles. The first is a crowded dark cloud containing circles of any diameter (i.e data of any N's) and lies at finite values of the $(\nabla \cdot \mathbf{u})$ relative norm. It corresponds to eigenmodes whose divergence does not vanish, with their associated eigenvalues converging with N towards a multiple integer of $-\pi^2/4$. A second cloud, much less loaded, expands below 10^{-2} in $(\nabla \cdot \mathbf{u})$ relative norm. It contains the genuine Stokes eigenmodes whose $(\nabla \cdot \mathbf{u})$ relative norm exponentially decreases with N, until reaching two different levels located at about 10^{-5} and 10^{-9}, as announced at the end of Section 7. The eigenvalues of the second cloud can be checked against the spectra obtained from the RH solver of the biharmonic problem (3) and (4). The regular drift of increasing $(\nabla \cdot \mathbf{u})$ relative norms, going from one cloud to the other, corresponds to the spatially under-resolved eigenmodes. As λ_k increases, with fixed N, the spatial resolution degrades and the clouds merge at some finite large $(\nabla \cdot \mathbf{u})$ relative norms, making it impossible to separate the genuine Stokes eigenmodes from the others.

All the $N = 16, 32, 48$ $\mathscr{L}$ eigenvalues are given in Fig. 5. If one excepts the tails where particular effects take place (commented below), an almost linear common behavior appears involving a large number of eigenvalues (a thousand of them for $N = 48$). The spectra contain few slightly complex eigenvalues, located only in the tails (see Fig. 1 of Section 4.1 in [22]), and represented here by their real part.

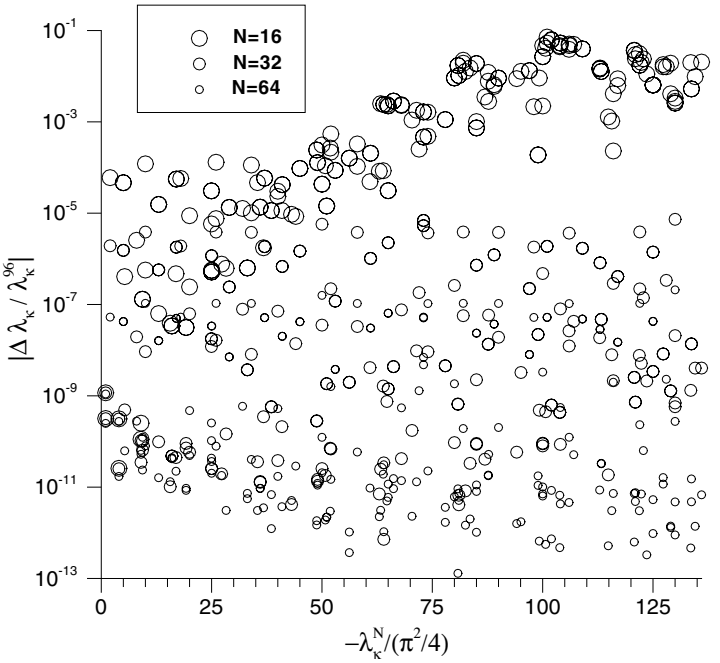

Fig. 3. The ratios $|\Delta\lambda_k/\lambda_k^{96}|$, with $\Delta\lambda_k = \lambda_k^{96} - \lambda_k^N$, as functions of $-\lambda_k^N/(\pi^2/4)$.

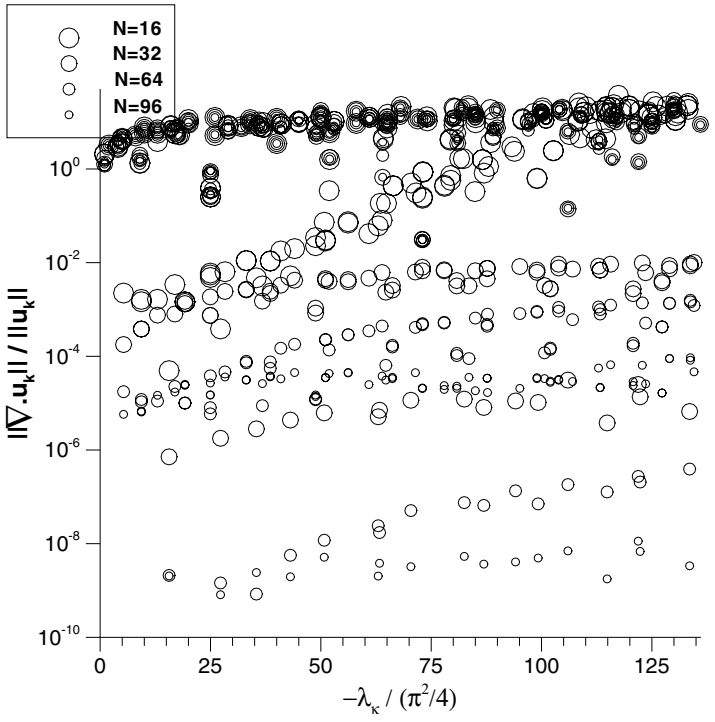

Fig. 4. The relative divergence norm, $\|\nabla \cdot \mathbf{u}_k\|/\|\mathbf{u}_k\|$, as function of $-\lambda_k^N/(\pi^2/4)$.

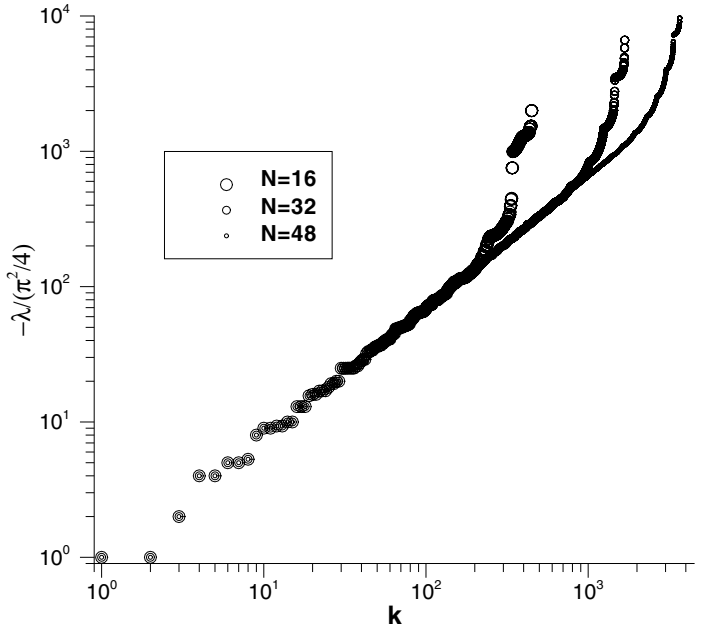

Fig. 5. All the $N = 16$, 32, 48 $\mathscr{L}$ eigenvalues $-\lambda_k^N/(\pi^2/4)$.

8.2. The Stokes eigenspace

8.2.1. The eigenvalues

The RH spectra obtained with $I = 63$ are shown in Fig. 6. They contain $I^2 = 3969$ modes $|-1,/,-1\rangle$, $I(I+1)/2 = 2016$ modes $|1,1,1\rangle$ and $|1,-1,-1\rangle$, and $I(I-1)/2 = 1953$ modes $|1,-1,1\rangle$ and $|1,1,-1\rangle$. Here again one observes a rapid increase of the extremal eigenvalues, while the remaining (major) part evolves almost linearly, in agreement with the asymptotic evaluation of [14], and thus corresponds to the true spectrum behavior. For the modes which are invariant under π-rotation, four families among the six, the slopes are approximately identical and twice larger than those of the $|-1,/,\pm1\rangle$ families. The fine structure of these spectra is illustrated in the enlargement. All these eigenvalues are unique, but they appear by sequences of packets of variable population within which they evolve more slowly than the global spectrum.

From the computed RH spectra, it is now possible to provide an empirical expression of their average behavior. From the analysis made in [14], to the leading linear law a $\sqrt{k}$ term might be added as a second order contribution. This is confirmed by our data. A systematic deflection from a linear law is indeed detected, except for the $|1,1,1\rangle$ family. Five laws, $t(k) = \sum_{l=1}^{L} \tau_l k^{1/l}$ with L going from 1 to 5, are thus tried and fitted with the Mathematica software on a part of the almost linear region, that is with the N_p data points indicated between parentheses in Table 1. The fits are appreciated by computing on $1.5N_p$ the relative deviations $E(k) = (t(k) - |\lambda_k - \lambda_1|)/|\lambda_k - \lambda_1|$. Table 1 gathers the results of the best fits of $-(\lambda_k - \lambda_1)$ for the $I = 15$, 31, 63 Galerkin–RH expansions. The λ_1's are listed in the first row of Table 2. For all but the first family of Table 1, a $\sqrt{k}$ contribution is required to get $E(k)$ distributions equally distributed around zero with a small amplitude. The second quantity quoted between parentheses in this table is $E = \max_{k \leqslant 1.5N_p} |E(k)|$. In all cases, E comes from the very beginning of the spectra. The other terms in $t(k)$ do not improve the fits.

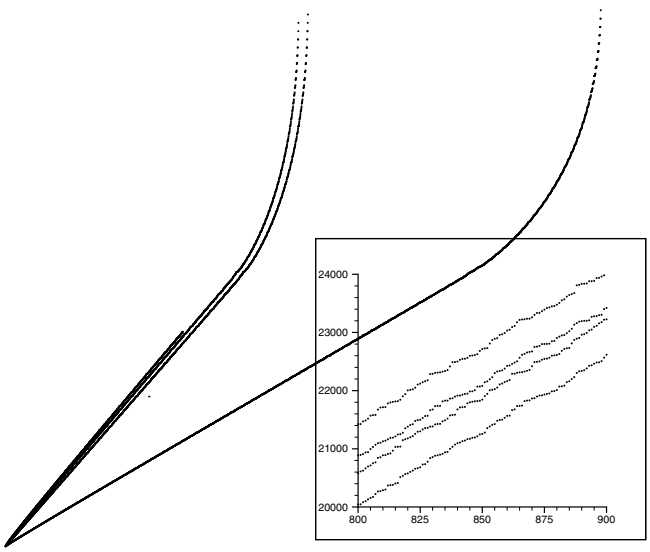

Table 1
The best fits of the Stokes spectra $-(\lambda_k - \lambda_1)$ for each symmetry family, with (N_p, E), respectively, the number of data points of the fit and the maximum relative error in the square, and of the fully periodic Stokes spectra

I	$\|1,1,1\rangle$	$\|1,-1,1\rangle$	$\|1,1,-1\rangle$	$\|1,-1,-1\rangle$	$\|-1,/,\pm1\rangle$
15	$\mathbf{25.0}k$	$20.1\sqrt{k} + \mathbf{25.9}k$	$34.6\sqrt{k} + \mathbf{26.4}k$	$13.7\sqrt{k} + \mathbf{25.7}k$	$12.7\sqrt{k} + \mathbf{12.8}k$
	(50, 0.06)	(50, 0.06)	(50, 0.06)	(50, 0.06)	(100, 0.06)
31	$\mathbf{25.0}k$	$23.3\sqrt{k} + \mathbf{25.3}k$	$40.2\sqrt{k} + \mathbf{25.5}k$	$16.0\sqrt{k} + \mathbf{25.3}k$	$14.3\sqrt{k} + \mathbf{12.6}k$
	(200, 0.02)	(200, 0.02)	(200, 0.02)	(200, 0.02)	(400, 0.015)
63	$\mathbf{25.1}k$	$24.9\sqrt{k} + \mathbf{25.2}k$	$43.5\sqrt{k} + \mathbf{25.2}k$	$17.2\sqrt{k} + \mathbf{25.2}k$	$15.2\sqrt{k} + \mathbf{12.6}k$
	(1000, 0.008)	(1000, 0.007)	(1000, 0.007)	(1000, 0.007)	(2000, 0.005)
62	$-31.5\sqrt{k} + \mathbf{25.1}k$	$-5.3\sqrt{k} + \mathbf{25.1}k$	$32.\sqrt{k} + \mathbf{25.2}k$	$5.6\sqrt{k} + \mathbf{25.1}k$	$\mathbf{12.6}k$
	(1000, 0.008)	(1000, 0.008)	(1000, 0.006)	(1000, 0.007)	(2000, 0.007)

Table 2
The seven fundamental Stokes eigenvalues $(-\lambda_k^{96})$ of each symmetry family, from the PrDi solver

k	$\|1,1,1\rangle$	$\|1,-1,1\rangle$	$\|1,1,-1\rangle$	$\|1,-1,-1\rangle$	$\|-1,/,\pm1\rangle$
1	13.086172791	38.531365767	67.280247001	32.052396078	23.031098494
2	41.757293817	87.329014683	125.25490397	69.769769316	47.392967028
3	61.581799188	106.35481679	155.42440823	100.96668085	61.580567435
4	90.687786716	156.16400139	203.55279952	127.97463234	81.660851437
5	108.69671662	173.68562127	232.20521027	157.61101251	95.076821486
6	150.21201788	214.44928129	283.39513465	206.15332909	120.42199692
7	159.67204918	244.84208020	301.84064257	209.72464870	125.98729896

The temporal decay rates of the four families $|1,\pm1,\pm1\rangle$ only differ by the $\sqrt{k}$ contribution. Their spectra have identical linear slopes which are twice as large as the linear slope of the $|-1,/,\pm1\rangle$ families. This important difference is a direct effect of the symmetry properties of these families. The four families $|1,\pm1,\pm1\rangle$ have the highest degree of symmetry. Being eigenmodes of the $\pi/2$-rotations, their wavenumber must increase in both x and y directions, giving the corresponding eigenvalues a faster growth than in the $|-1,/,\pm1\rangle$ families.

Let us consider the *fully periodic* Stokes eigenmodes of wavelength equal to two (the square characteristic size), written for each symmetry family according to:

$$|1,1,1\rangle \div \cos(m\pi x)\cos(n\pi y) + \cos(n\pi x)\cos(m\pi y), \quad m \geqslant n = 0,\ldots,I,$$

$$|1,-1,1\rangle \div \cos(m\pi x)\cos(n\pi y) - \cos(n\pi x)\cos(m\pi y), \quad m > n = 0,\ldots,I,$$

$$|1,1,-1\rangle \div \sin(m\pi x)\sin(n\pi y) - \sin(n\pi x)\sin(m\pi y), \quad m > n = 1,\ldots,I,$$

$$|1,-1,-1\rangle \div \sin(m\pi x)\sin(n\pi y) + \sin(n\pi x)\sin(m\pi y), \quad m \geqslant n = 1,\ldots,I,$$

$$|-1,/,1> \div \sin(m\pi x)\cos(n\pi y), \quad m = 1,\ldots,I,\ n = 0,\ldots,I,$$

$$|-1,/,-1\rangle \div \cos(m\pi x)\sin(n\pi y), \quad m = 0,\ldots,I,\ n = 1,\ldots,I.$$

The corresponding spectra can be exactly computed and are shown in Fig. 7 for $I = 62$. They exhibit very similar behaviors to those given in Fig. 6: they contain an almost linear part and a rapidly increasing tail. Fitting the linear part, with the previously mentioned method, provides the results presented in the last row of Table 1. Here $\lambda_1 = 0, \pi^2, 5\pi^2, 2\pi^2, \pi^2, \pi^2$ for the successive symmetry families. The linear parts of the confined and fully periodic Stokes eigenmodes spectra are in excellent agreement. They only differ by the $\sqrt{k}$ contributions which are important to describe the beginning of the spectra. It can thus be inferred that the confinement merely affects this contribution in the Stokes eigenmodes spectra.

The 1D confined Stokes eigenmodes cannot be considered with all these symmetry families, since by definition they have no $\pi/2$-rotation symmetry. They only pertain to the $|-1,/,\pm 1\rangle$ families described by the following stream function expressions:

$$\left(\frac{\cosh(n\pi x)}{\cosh(n\pi)} - \frac{\cos(\mu_{\text{even}} x)}{\cos(\mu_{\text{even}})}\right)\sin(n\pi y), \quad \left(\frac{\sinh(n\pi x)}{\sinh(n\pi)} - \frac{\sin(\mu_{\text{odd}} x)}{\sin(\mu_{\text{odd}})}\right)\cos(n\pi y).$$

Computing the spectra is not straightforward. Their asymptotic evolution, by ordering in λ_k, is also mainly linear and described by the respective sequences of eigenvalues $[(2m+1)^2 + (2n)^2](\pi^2/4)$ and $[(2m)^2 + (2n)^2](\pi^2/4)$, with the linear slope 12.6 already encountered with this family.

All these results suggest that the asymptotic spectra per symmetry family of the Stokes eigenmodes follow specific evolution laws, whether they be confined or not.

Finally, the observed behavior of the tails in the numerical spectra is now briefly discussed. This behavior is due to two effects: firstly, the cut-off influence on a 2D spectrum ordered by increasing eigenvalues, also present in the analytical periodic spectrum. A second contribution is expected from pure numerical truncation effects, as already observed and analytically verified with the numerical d^2/dx^2 spectrum (cf. [39,15, Fig. 2.7.2. p. 81]).

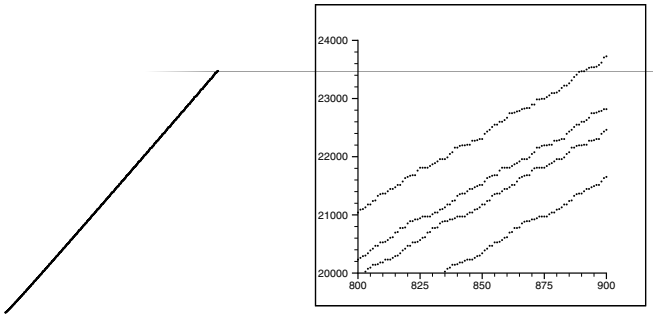

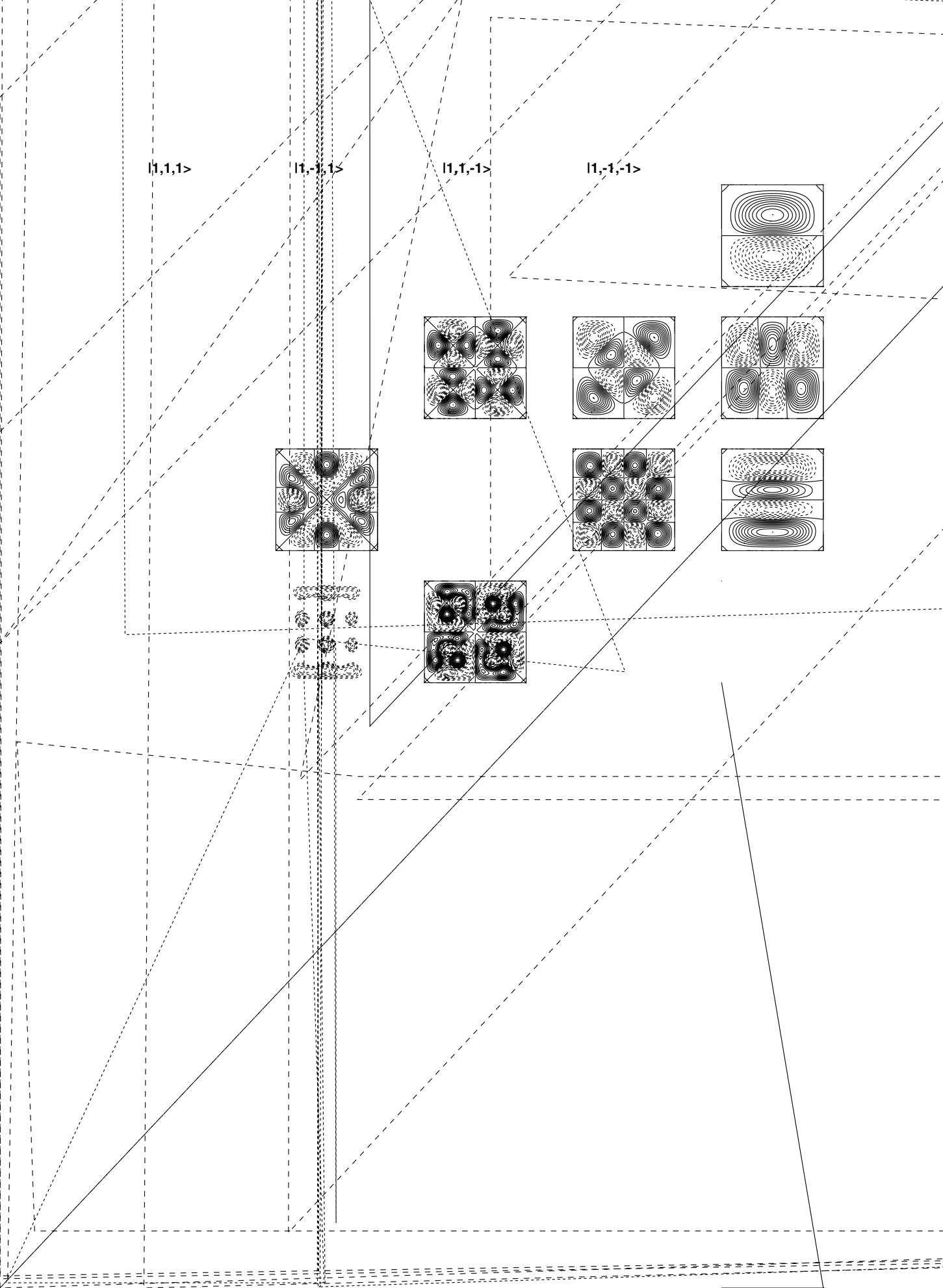
|1,1,1>
|1,-1,1>
|1,1,-1>
|1,-1,-1>

8.2.2. The eigenmodes

Figs. 8 and 9, respectively, show the stream function $\psi_k(x,y)$ and the normalized vorticity $\omega_k(x,y)/|\lambda_k|$ contour lines of the first seven eigenmodes in each symmetry family, their corresponding eigenvalues being listed in Table 2. These data come from the $N = 96$ PrDi solver. The stream functions are normalized in such a way that the largest nodal value is set to one. These charts are not intended to exhibit the corner eddies (see [23]) whose existence in our numerical fields is simply suggested by a tiny $\psi = 0$ contour in each corner in Fig. 8, and attested to by the enlargements in Fig. 2 made from the contour plots of the fundamental $|1,1,1\rangle$, $|1,-1,1\rangle$ and $|-1,/,-1\rangle$ eigenmodes. The first two modes have opposite reflection symmetry properties about the square diagonals, and the third one does not show this property although it appears as mainly symmetrical (see Section 7). The size of the corner eddies is seen to decrease with increasing $|\lambda_k|$.

As expected, the largest is $|\lambda_k|$ the highest is the number of elementary patterns (structures), or in other words, the highest is the "average wavenumber" of the ψ and ω fields.

Albeit simple a priori, the dynamics underlying the eigenmodes behavior deserves to be described with some details. To this end, Fig. 10 shows the contour lines of each component of $\mathbf{u}$, $\mathbf{\Delta u}$ and ∇p of the 3rd $|1,-1,-1\rangle$ eigenmode, three quantities which must be balanced according to Eq. (2). Two regions of the flow are considered. The first one, denoted by $\mathscr{R}_B$, is a layer going along the boundaries in which the pressure gradient is important, and the second, $\mathscr{R}_C$, is the core where this gradient gets very small. The $\mathscr{R}_B$ layers get thinner and thinner as $|\lambda_k|$ increases. The reason why the pressure gradient is so confined near the boundaries is contained in the system (7): by Eq. (11) the pressure along the boundaries is almost periodic (see the $\mathbf{\Delta u}$ contour lines) and its harmonicity makes it exponentially decreasing going away from them, more and more stiffly with increasing $|\lambda_k|$.

Consequently, a specific dynamic equilibrium prevails in each region. In $\mathscr{R}_B$ the velocity amplitude vanishes and the balance is expressed by the condition (11). In $\mathscr{R}_C$ the balance is isobaric, given by $\lambda\mathbf{u} = \mathbf{\Delta u}$, as in the fully periodic case (see Eq. (5)). This is what one sees by comparing the $\lambda\mathbf{u}$ and $\mathbf{\Delta u}$ contour plots in the flow core.

Then comes a relationship verified by any 2D flow, steady or not, confined or not, namely $(\mathbf{\Delta u}\cdot\nabla)\omega \equiv 0$ from which it is straightforward to check that $\lambda(\mathbf{u}\cdot\nabla)\omega = 0$ in $\mathscr{R}_C$: this implies that the vorticity is conserved along the Stokes eigenmodes stream lines in $\mathscr{R}_C$. In other words, there exists a relationship $\omega = f(\psi)$ which must be linear in the Stokes problem. Moreover, this slope is equal to $-\lambda$ as expected from the buckling load equation which can be derived from $\omega(x,y) = -\mathbf{\Delta}\psi = -\lambda\psi$. The same relation holds in the case of the fully periodic situation. The confirmation is provided by comparing in $\mathscr{R}_C$ the ψ and ω contours in Figs. 8 and 9, for each eigenmode. The effective (ψ, ω) correlation is given in Fig. 11, obtained defining arbitrarily $\mathscr{R}_C$ to be $[-0.6,0.6]^2$, and normalizing the vorticity by the corresponding $-\lambda_k$. Although the relationship $\omega = -\lambda\psi$ is expected to be better verified with larger $|\lambda|$'s, it clearly underlies all these graphs, almost exactly for some of them including the most fundamental ones, whilst for others it is slightly scattered and generates a zigzag path around $\omega = -\lambda\psi$.

The relationship $\omega = -\lambda\psi$ can then be taken as specific to the particular dynamics of the 2D Stokes eigenmodes.

By careful inspection of the contour plots within the regions $\mathscr{R}_C$ in Figs. 8 and 9, where the ratio ω/ψ is constant and positive, one can see the $\omega = 0$ contour line. It often closely follows the square boundary. This contour can certainly be considered as the extreme outer border of $\mathscr{R}_C$, whose area grows with $|\lambda|$ per symmetry family.

A functional relationship between the stream function and the vorticity of steady 2D confined flows at high Reynolds number was suggested a long time ago by Batchelor [3,4, p. 536] to characterize the inviscid regions. Beside the few attempts quoted in [37,38] to identify this relationship, it has been proposed in [37,38] that a functional relationship could also exist for the Stokes eigenmodes. The first five fundamental modes in the square were therein published, namely the first three $|1,1,1\rangle$ and two $|1,-1,1\rangle$ eigenmodes of

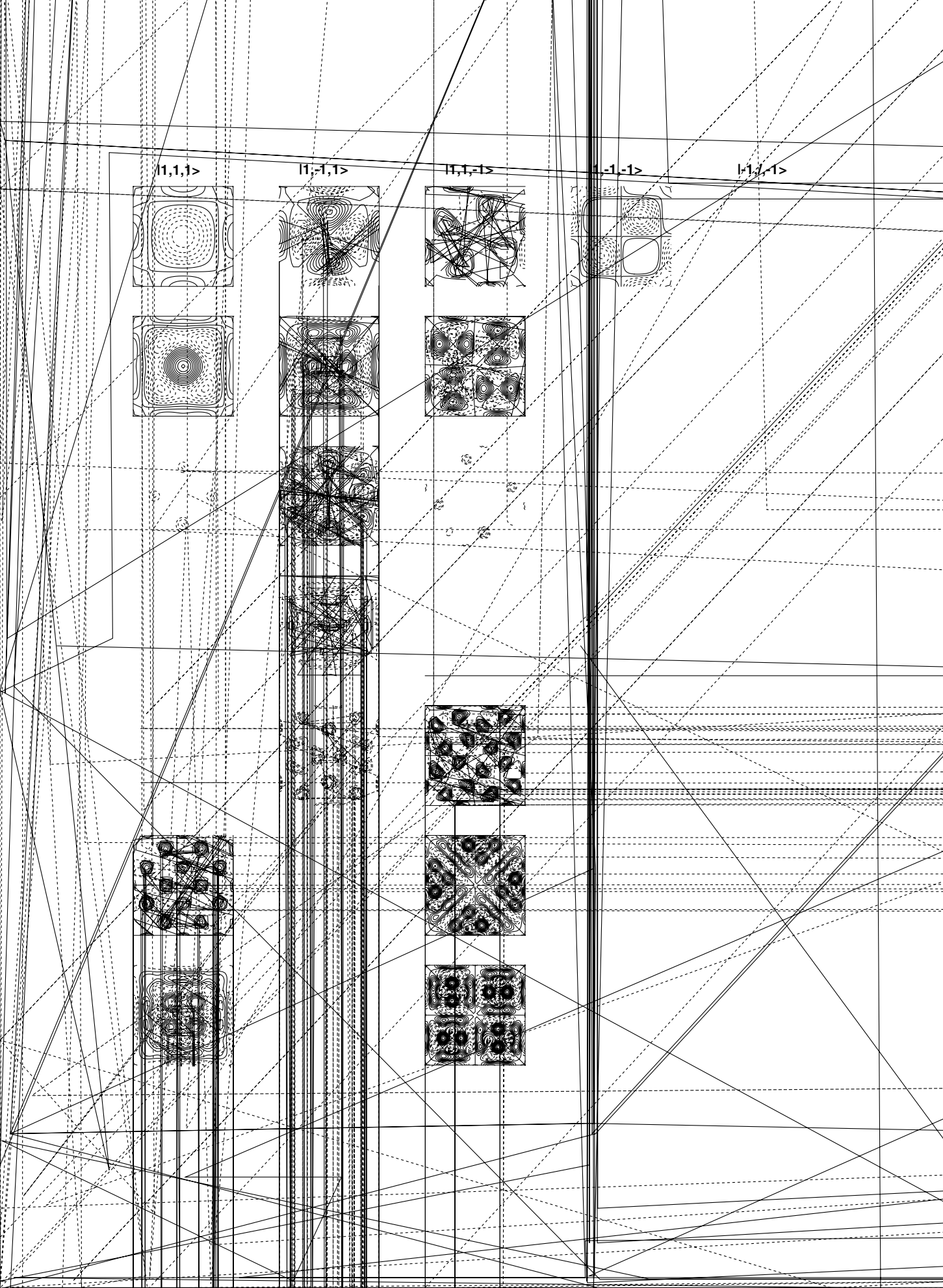
|1,1,1>
|1,-1,1>
|1,1,-1>
|1,-1,-1>
|-1,1,-1>

Fig. 11. The (ψ, ω) correlation obtained in $\mathscr{R}_C = [-0.6, 0.6]^2$ for the first seven eigenmodes of each symmetry family.

Table 2. The linear correlation was detected only for the most fundamental one. It is therefore clearly settled now that a linear relationship does exist between the stream function and the vorticity in the core of all the Stokes eigenmodes in the square.

This is a definite answer, and conclusion, to the discussion developed in [4, p. 537], where Batchelor writes "Thus a solution for ψ as a function of x and y obtained from $-\omega = \Delta\psi = \lambda\psi$ represents either a steady motion of an inviscid fluid, or, when multiplied by $\exp(-\lambda t)$, a decaying motion of viscous fluid". In fact the linear relationship is verified in the core of the Stokes eigenmodes in the square (and presumably in any closed geometry), while this relation should be nonlinear for the inviscid dynamics. Moreover, it is worth noticing that the well-known Bernouilli relation $\mathbf{u} \times \vec{\omega} = \nabla H$ characterizing the "total head" H gradient in the inviscid regions has a "viscous partner" for each Stokes eigenmode within $\mathscr{R}_C$, namely $\mathbf{u} \times \vec{\omega} = (\lambda/2)\nabla\psi^2$.

The above described dynamics must hold for the 3D Stokes eigenmodes, in the cube for instance. The pressure will again tend to zero far from the walls, where the momentum balance remains essentially governed by $\lambda\mathbf{u} = \boldsymbol{\Delta}\mathbf{u}$. But $(\boldsymbol{\Delta}\mathbf{u} \cdot \nabla)\vec{\omega} \neq 0$ in 3D flows.

9. Conclusions

Two different solvers have been used to compute the Stokes eigenmodes in the square, a (velocity, pressure) PrDi solver based on a Chebyshev collocation scheme and a Galerkin–RH expansion for the Stokes stream function formulation. The former solver supplies genuine Stokes eigenmodes whose divergence cancels asymptotically with the grid refinement, distributed among many eigenmodes of another system, the divergence diffusion problem. From both solvers comes the complete identification of the Stokes eigenmodes in the square for each of the six symmetry families which can be defined in the square. The spectra $-\lambda_k$ are asymptotically linear in k, but contain, for all but one symmetry family, a significant contribution in $\sqrt{k}$. The existence of both these terms was theoretically predicted in [14]. The slopes are sensitive to the symmetries. In particular, the linear growth of the spectra in the four symmetry families which are invariant under the π-rotation is twice as large as that of the other two families. Two dynamic equilibria govern the eigenmodes velocity fields. The first occurs along the boundaries where the pressure gradient compensates the momentum diffusion, as in a Poiseuille flow. The second occurs in the core where the equilibrium is isobaric. In this region a linear relationship occurs between the vorticity and the stream function of each eigenmode, $\omega = -\lambda\psi$, leading to $\mathbf{u} \times \vec{\omega} = (\lambda/2)\nabla\psi^2$, a "viscous" relation which echoes the total head gradient one of the inviscid parts of the high Reynolds number flows. Therefore, the confined 2D flows enjoy the property of having their vorticity in functional relationship with the stream function, in both viscous and inviscid regimes. This was suggested more than 30 years ago by Batchelor [4].

The knowledge and interpretation of the Stokes eigenmodes in the square should thus bring an interesting point of view over the resulting dynamics of 2D closed flows, complementary to what is well known regarding the inviscid regions. Analyzing the 3D Stokes eigenmodes, in the cube for instance, will likely provide valuable understanding elements on realistic flows.

Acknowledgements

The authors thank Prof. M.O. Deville for helpful discussions. The second author gratefully acknowledges the financial support from the ERCOFTAC visitor programm sponsored by the L. Euler Pilot Center (Switzerland) at EPFL, and the FSTI-EPFL for the Invited Professor Fellowship. The computing resources were made available by CSCS, Manno, Switzerland. The authors thank Dr. N. Borhani (LMF-ISE-FSTI-EPFL) for proof reading the manuscript.

References

[1] MATLAB, 2002. Available from <http://www.mathworks.com/>.
[2] K. Arrow, L. Hurwicz, H. Uzawa, Studies in Nonlinear Programming, Stanford University Press, Stanford, 1968.
[3] G.K. Batchelor, On steady laminar flow with closed streamlines at large Reynolds number, J. Fluid Mech. 1 (1956) 177–190.
[4] G.K. Batchelor, An Introduction to Fluid Dynamics, Cambridge University Press, Cambridge, 1967 (reprinted 1994).
[5] P.F. Batcho, G.E.M. Karniadakis, Generalized stokes eigenfunctions: a new trial basis for the solution of the incompressible Navier–Stokes equations, J. Comput. Phys. 115 (1994) 121–146.
[6] B. Bialecki, A. Karageorghis, A Legendre spectral collocation method for the biharmonic Dirichlet problem, ESAIM – Math. Model. Numer. Anal. – Modélisation Mathématique et Analyse Numérique 34 (3) (2000) 637–662.
[7] B. Bialecki, A. Karageorghis, A Legendre spectral Galerkin method for the biharmonic Dirichlet problem, SIAM J. Sci. Comput. 22 (5) (2001) 1549–1569.
[8] P.E. Bjørstad, B.P. Tjøstheim, Efficient algorithms for solving a fourth-order equation with the spectral-Galerkin method, SIAM J. Sci. Comput. 18 (2) (1997) 621–632.
[9] P.E. Bjørstad, B.P. Tjøstheim, High precision solutions of two fourth order eigenvalue problems, Computing 63 (2) (1999) 97–107.
[10] O. Brodier, T. Neicu, A. Kudrolli, Eigenvalues and eigenfunctions of a clover plate, Eur. Phys. J. B 23 (3) (2001) 365–372.
[11] B.M. Brown, E.B. Davies, P.K. Jimack, M.D. Mihajlovic, A numerical investigation of the solution of a class of fourth-order eigenvalue problems, Proc. R. Soc. Lond. A 456 (2000) 1505–1521.
[12] C. Canuto, M.Y. Hussaini, A. Quarteroni, T.A. Zang, Spectral Methods in Fluid Dynamics, Springer Series in Computational Physics, Springer, New York, 1988.
[13] H.J.H. Clercx, S.R. Maassen, G.J.F. van Heijst, Decaying two-dimensional turbulence in square containers with no-slip or stress-free boundaries, Phys. Fluids 11 (3) (1999) 611–626.
[14] P. Constantin, C. Foias, Navier–Stokes Equations, Chicago Lectures in Mathematics, University of Chicago Press, Chicago, 1988.
[15] M.O. Deville, P.F. Fischer, E.H. Mund, High-order Method for Incompressible Fluid Flow, Cambridge University Press, Cambridge, 2002.
[16] P.H. Gaskell, J.L. Summers, H.M. Thompson, M.D. Savage, Creeping flow analyses of free surface cavity flows, Theoret. Comput. Fluids Dyn. 8 (1996) 415–433.
[17] D. Gottlieb, S.A. Orszag, Numerical Analysis of Spectral Methods: Theory and Applications, SIAM-CBMS, Philadelphia, 1977.
[18] D.L. Harris, W.H. Reid, On orthogonal functions which satisfy four boundary conditions. I. Tables for use in Fourier-type expansions, Astrophys. J. Supp. Ser. 3 (1958) 429–447.
[19] L. Kleiser, U. Schumann, Treatment of the incompressibility and boundary conditions in 3-D numerical spectral simulation of plane channel flows, in: E.H. Hirschel (Ed.), Proceedings of the 3th GAMM Conference on Numerical Methods in Fluid Mechanics, Vieweg, Braunschweig, 1980, p. 165.
[20] G. Labrosse, E. Tric, H. Khallouf, M. Betrouni, A direct (pseudo-spectral) solver of the 2D/3D Stokes problem: transition to unsteadiness of natural convection flow in a differentially heated cubical cavity, Numer. Heat Transfer B (31) (1997) 261–276.
[21] R.B. Lehoucq, D.C. Sorensen, C. Yang, ARPACK Users' Guide, SIAM, Philadelphia, 1998.
[22] E. Leriche, G. Labrosse, High-order direct Stokes solvers with or without temporal splitting: numerical investigations of their comparative properties, SIAM J. Sci. Comput. 22 (4) (2000) 1386–1410.
[23] E. Leriche, G. Labrosse, Fundamental Stokes eigenmodes in the square: which expansion is more accurate, Chebyshev or Reid-Harris? Numer. Algorithms (2004), to appear.
[24] H.K. Moffatt, Viscous and resistive eddies near a sharp corner, J. Fluid Mech. 18 (1964) 1–18.
[25] S.A. Orszag, M. Israeli, M. Deville, Boundary conditions for incompressible flows, J. Sci. Comput. 1 (1) (1986) 75–111.
[26] W.H. Reid, D.L. Harris, On orthogonal functions which satisfy four boundary conditions. II. Integrals for use with Fourier-type expansions, Astrophys. J. Supp. Ser. 3 (1958) 448–452.
[27] M. Schumack, W. Schultz, J. Boyd, Spectral method solution of the Stokes equations on nonstaggered grids, J. Comput. Phys. 94 (1991) 30–58.
[28] I.H. Shames, C.L. Dym, Energy and Finite Element Methods in Structural Mechanics, McGraw-Hill, New York, 1985.
[29] P.N. Shankar, The eddy structure in stokes flow in a cavity, J. Fluid Mech. 250 (1993) 371–383.
[30] J. Shen, Efficient spectral-Galerkin method. Part 1: direct solvers of 2nd-order and 4th-order equations using Legendre polynomials, SIAM J. Sci. Comput. 15 (6) (1994) 1489–1505.
[31] J. Shen, Efficient spectral-Galerkin method. Part 2: Direct solvers of 2nd-order and 4th-order equations using Chebyshev polynomials, SIAM J. Sci. Comput. 16 (1) (1995) 74–87.
[32] J. Sivardière, La Symétrie en Mathématique, Physique et Chimie, Presses Universitaires de Grenoble, Grenoble, 1995.
[33] R.C.T. Smith, The bending of a semi-infinite strip, Aust. J. Sci. Res. 5 (1952) 227–237.
[34] L. Sturges, D.D. Joseph, The free surface on a simple fluid between cylinders undergoing torsional oscillations. Part III: oscillating planes, Arch. Rat. Mech. Anal. 64 (1977) 245–267.

[35] G.I. Taylor, The buckling load for a rectangular plate with four clamped edges, Ztschr. f. Angew. Math. Mech. 13 (2) (1933) 147–152.
[36] B.P. Tjøstheim, A study of fourth order elliptic problems with constant coefficients in two and three dimensions, Ph.D. Thesis, University of Bergen, 2000.
[37] J.A. van de Konijnenberg, Spin-up in non-axisymmetric containers, Ph.D. Thesis, Eindhoven University of Technology, 1995.
[38] J.A. van de Konijnenberg, J.B. Flor, G.J.F. van Heijst, Decaying quasi-two-dimensional viscous flow on a square domain, Phys. Fluids 10 (3) (1998) 595–606.
[39] H. Vandeven, On the eigenvalues of the second-order spectral differentiation operators, Comput. Meth. Appl. Mech. Eng. 80 (1990) 313–318.
[40] S. Wolframm, Mathematica. A System for Doing Mathematics by Computer, Addison-Wesley, New York, 2000.